JOURNAL OF MATERIALS SCIENCE 31 (1996) 3333–3347

Review
Micromechanical and thermodynamical aspects of environmental crazing

M. KOTOUL*
Department of Materials Engineering, University College of Swansea, Swansea SA2 8PP, UK

The present study aims 1) to investigate theoretically the relation between the craze microstructure and the basic materials parameters such as the yield stress and the surface energy and 2) to provide a detailed thermodynamic treatment of a single isolated craze in glassy polymer tested in an aggressive liquid environment. Based on the assumption that the craze tip is somewhat blunted by small scale yielding and on the Taylor meniscus instability as the mechanism responsible for the propagation of the leading edge of the craze, the detailed micromechanical analysis is used to provide estimates of the critical opening displacement of the craze for growth initiation, mean fibril spacing, mean fibril diameter and fibril volume fraction at the craze tip. The influence of aggressive liquid environments on the yield stress and the surface energy is discussed together with predicted changes in the craze microstructure. The thermodynamic analysis starts with the recognition that induced high negative pressures around the craze tip can increase the solubility of a liquid at this site by several orders of magnitude. As a consequence the local density of thermodynamic potential drops significantly. This unbalanced fall in thermodynamic potential provides an additional driving force for the craze advance. It is shown that a corresponding release of external load is required to preserve the overall balance of the specimen with craze.

I. Introduction

It is a matter of record that many polymeric materials loaded mechanically and immersed in certain kinds of liquid undergo much more readily failures by crazing and/or cracking than in air conditions [1, 2]. It should be noted that the failure promoting liquids are very often non solvents and chemically inert for polymers. This phenomenon, generally called "environmental stress cracking" (ESC), has been subjected to intensive experimental and theoretical [3–7] research in the past two decades because of its serious consequences in engineering structures.

Substantial work has been devoted to the mechanism of craze initiation at imperfections generally present at the interface of a stressed or strained polymer in certain liquid environments and also to the mechanism of subsequent growth [8, 9].

On a molecular level the effect of aggressive liquids and gasses is observed in changes in the spectrum of relaxation times. A reduction in the relaxation time associated with the collective motion of molecular segments results in a decrease in stiffness of the material. Agents having this influence are usually termed plasticizers.

The known experimental data base clearly demonstrate that crazing agents reduce the resistance to plastic deformation. The two main modes of action which have been envisaged for crazing agents are; (i) the depression of the glass transition temperature, T_g, i.e. the plasticization of the material, and (ii) the reduction of the surface energy of the craze fibrils. The depression of T_g has usually been approximated in terms of the concentration of the absorbed crazing agent in the polymeric material by formula

$$T_g(\varphi) = 0.63\varphi T_m + (1 - \varphi)T_g(0), \qquad (1)$$

where φ is the concentration of absorbed crazing agent, T_m is the melting temperature of the absorbed component and $T_g(0)$ is the glass transition temperature of the pure amorphous polymer ($\varphi = 0$). The reduction of the resistance to plastic deformation can then be described using the results obtained for PMMA by Ward [10] who proposed a simple relationship between the yield stress and the glass-temperature

$$\sigma_Y(\varphi, T) = \sigma_Y(0, T)\frac{T_g(\varphi) - T}{T_g(0) - T}, \qquad (2)$$

Permanent Address: Department of Solids Mechanics, Technical University of Brno, Technicka 2, Brno 616 69, Czech Republic, address where any correspondence should be sent.

0022–2461

in which $T_g(0)$ and $T_g(\varphi)$ are defined as in Equation 1, T is the actual temperature and $\sigma_Y(0, T)$ represents the yield stress of the pure amorphous polymer at this temperature.

It is a matter of long dispute whether the reduction of the resistance to plastic deformation or the reduction of the surface energy is more important in promoting ESC. For a long time the plasticization has been considered to be more dominant. Namely, the reduced resistance to molecular motion caused by the plasticization should facilitate the formation of voids, which then develop into crazes and also should facilitate crack propagation. It would, however, also be expected to lower the yield stress and make shear yielding easier. This leads to the possible dilemma as to why a reduction in yield stress produces a more brittle behaviour. It is the goal of this paper to shed some light on this problem.

In addition we will also address the changes in craze microstructure due to the environment, particularly at the craze tip. Two characteristics of the craze microstructure, i.e. the mean fibril diameter, $\bar{D}$, and the mean fibril spacing will be investigated theoretically. So far these characteristics have been obtained only experimentally using transmission electron microscopy, small-angle X-ray and small-angle neutron scattering. It was found [2] that the presence of a crazing agent generally results in coarser craze fibrils and a greater mean fibril spacing.

2. Analysis

The analysis consists of two main sections. In the first section a micromechanical analysis of the leading edge of a craze is provided with the aim of deriving a critical displacement at the craze tip, h_{crit}, which ensures the initiation of craze advance. An estimate of the mean fibril diameter and the mean fibril spacing will also be given.

The second section deals with a thermodynamic analysis of a single craze in a polymer sample immersed in a certain kind of liquid and subjected to a deformation or load. The craze growth will be interpreted in terms of a disturbance of the thermodynamic equilibrium rather than the normally considered mechanical equilibrium. In terms of the thermodynamics the immersed polymeric material is treated as an open system, i.e. a system in which mass may be transported to or from surroundings. A thermodynamic force resulting from the thermodynamic non-equilibrium between the polymer sample and the environment plays the role of an additional driving force for the craze growth. It is suggested that the traditional fracture mechanics approach has to be extended to incorporate "other loading mechanisms" of non-mechanical, i.e. chemical, origin in order to assess the craze stability satisfactorily. The critical displacement derived in the first section is later applied in the course of the thermodynamic analysis. Note that since the quasi-static initiation of craze growth is addressed, all rate effects will be omitted.

2.1. Micromechanics of craze advance

In a series of papers Argon and Salama [11, 12] developed a mechanism for the propagation of the leading edge of the craze that utilized the so-called Taylor meniscus instability [13]. Remarkable experimental confirmation of this process has been given by Donald and Kramer [14].

It is argued that the craze tip is somewhat blunted by small scale yielding. The interface between the craze and uncrazed polymer is considered to have a sinusoidal perturbation of wavelength Λ of the following form, see Fig. 1

$$x = x_0 + C \sin \frac{2\pi z}{\Lambda}. \tag{3}$$

The interface is moving under a hydrostatic stress gradient dp/dx. The perturbation introduces a radius of curvature $P = \Lambda^2/4\pi^2 C$, which because of the surface energy Γ causes a hydrostatic stress necessary to increase the perturbation. It was shown [12, 15] that the fastest growing wavelength Λ_f is $3^{1/2}\Lambda_m$ where Λ_m is the minimum wavelength for the perturbation to grow

$$\Lambda_m = (\Gamma/(dp/dx))^{1/2}. \tag{4}$$

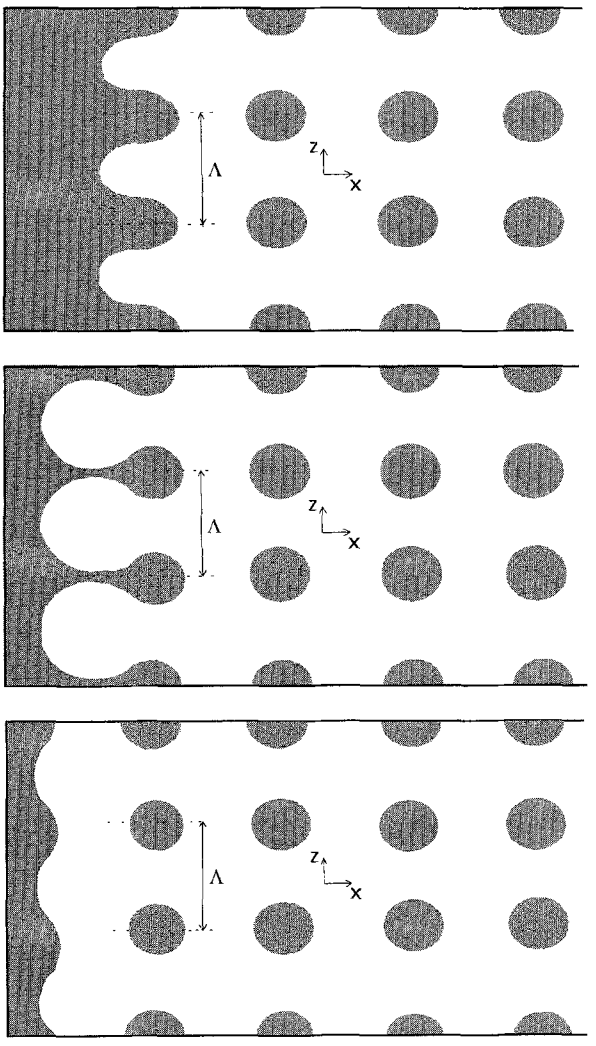

Figure 1 A schematic representation of the process of fibril formation at the advancing craze tip

For an ideally plastic material neglecting all rate effects, Λ_f is given by the simple formula

$$\Lambda_f = \pi\left(\frac{6\Gamma h}{\tau_0}\right)^{1/2}, \tag{5}$$

where h is the opening displacement at the craze tip and τ_0 is the yield stress in shear.

2.1.1. Theoretical model

Accepting the Taylor meniscus instability as the mechanism for propagation of the leading edge of the craze, we will first try to describe the growth in the perturbation. With reference to Fig. 1, we assume that the perturbation grows by a simultaneous increase in amplitude and expansion of void "fingers" like a cylindrical cavity in the surrounding stress–strain field. The convolution of the leading craze edge must induce the perturbation of the strain field some distance ahead of craze tip. If initially, the state of plane-strain prevailed at some point ahead of the craze tip, this ceases to be true as the perturbed craze tip approaches this point because the condition of plane strain $\varepsilon_z = 0$ cannot be sustained any longer since the material is being redistributed along the leading craze edge. It is matter of interest to find a point where the unperturbed and perturbed field match each other. Note that a similar problem was discussed by Argon and Salama [11].

The distribution of radial and tangential strain rates in terms of the uniform axial strain rate $\dot{\varepsilon}_y$ (the y-axis is chosen now as the axis of cylindrical symmetry) and the strain rate $\dot{r}_0/r_0$ at the inner radius r_0 of a cylindrical hole are well-known [16, 17]:

$$\dot{\varepsilon}_r = -\frac{r_0^2}{r^2}\left(\frac{\dot{r}_0}{r_0} + \frac{\dot{\varepsilon}_y}{2}\right) - \frac{\dot{\varepsilon}_y}{2}, \tag{6}$$

$$\dot{\varepsilon}_\theta = \frac{r_0^2}{r^2}\left(\frac{\dot{r}_0}{r_0} + \frac{\dot{\varepsilon}_y}{2}\right) - \frac{\dot{\varepsilon}_y}{2}. \tag{7}$$

It follows from Equation 7 that there exists a radius r where $\dot{\varepsilon}_\theta = 0$ for $\dot{r}_0 > 0$. We adopt Equations 6 and 7 to approximate the perturbed field ahead of the corrugated craze tip bearing in mind their highly approximate character because of the non uniformity of the axial strain rate $\dot{\varepsilon}_y$ and interaction between neighbouring void "fingers". Following McClintock's [17] extrapolation to elliptical holes, we identify $\dot{r}_0/r_0$ with the mean radius growth rate $\dot{\mathfrak{R}}/\mathfrak{R}$ for which the following equation holds [17]

$$\frac{\dot{\mathfrak{R}}}{\mathfrak{R}} = \frac{\dot{\bar{\varepsilon}}3^{1/2}}{2}\sinh\left(\frac{3^{1/2}}{2}\frac{(\sigma_a + \sigma_b)}{\bar{\sigma}}\right) + \frac{\dot{\varepsilon}_a + \dot{\varepsilon}_b}{2}, \tag{8}$$

where ε_a, ε_b, σ_a, σ_b are remote strains and stresses in the plane perpendicular to the cylindrical axis y, $\bar{\varepsilon}$ is the equivalent strain defined as

$$\bar{\varepsilon} = \left\{\frac{2}{9}\left[(\varepsilon_a - \varepsilon_b)^2 + (\varepsilon_b - \varepsilon_y)^2 + (\varepsilon_y - \varepsilon_a)^2\right]\right\}^{1/2} \tag{9}$$

and $\bar{\sigma}$ is the equivalent Mises yield stress

$$\bar{\sigma} = 3^{1/2}\tau_0, \tag{10}$$

where τ_0 is again the yield stress in shear. Because of the plane strain conditions $\varepsilon_b \equiv 0$ and $\varepsilon_a = -\varepsilon_y$, thus

$$\bar{\varepsilon} = \frac{2}{3^{1/2}}\varepsilon_y. \tag{11}$$

The values of σ_a and σ_b are estimated from the results of an exponential slip line field ahead of a semicircular notch tip [18], assuming the same kind of field ahead of the blunted craze tip. This provides

$$\frac{\sigma_a + \sigma_b}{2} = 2\tau_0\left(\frac{1}{4} + \log\frac{2\xi}{h}\right), \tag{12}$$

where ξ is measured from the notch tip centre curvature with the radius $h/2$. The maximum value of $(\sigma_a + \sigma_b)/2$ is achieved at $\xi = h/2\exp(\pi/2)$ when the spiral region completely envelopes the semicircular tip giving

$$\frac{\sigma_a + \sigma_b}{2} = 2\tau_0\left(\frac{1}{4} + \frac{\pi}{2}\right). \tag{13}$$

Substituting Equations 10, 11 and 13 into Equation 8 we get

$$\frac{\dot{\mathfrak{R}}}{\mathfrak{R}} = \dot{\varepsilon}_y \sinh\left(\frac{1}{2} + \pi\right) - \frac{\dot{\varepsilon}_y}{2}, \tag{14}$$

or, accounting for the effect of surface tension

$$\frac{\dot{\mathfrak{R}}}{\mathfrak{R}} = \dot{\varepsilon}_y \sinh\left(\frac{1}{2} + \pi - \frac{\Gamma}{\tau_0\mathfrak{R}}\right) - \frac{\dot{\varepsilon}_y}{2}. \tag{15}$$

Before substituting Equation 14 or Equation 15 into Equation 7 we need to know an initial local "porosity" $\alpha \approx (2r_0/\Lambda_f)^2$, or the initial value of r_0 in Equations 6 and 7. This is a rather arbitrary element of the analysis. In the work of Argon and Salama [11] the value $\alpha \approx 0.1$ is considered. This value may be easily justified by the consideration that the radius of curvature of the perturbation $P = \Lambda_f^2/4\pi^2 C$ decreases with increasing amplitude C of the perturbation. At the moment when $P = C$, the perturbation is quite well developed, and half the wavelength of a sine curve may be approximated by a semicircle. The perturbed strain field ahead of the corrugated craze tip may be approximated by Equations 6 and 7 and as a consequence of local applied stress and strain the curvature radius again increases due to the expansion of void "fingers", Identifying P with r_0 at the moment when $P = C$ we get

$$r_0 = \frac{\Lambda_f}{2\pi} = \frac{1}{2}\left(\frac{6\Gamma h}{\tau_0}\right)^{1/2}, \tag{16}$$

which gives the porosity $\alpha \approx \left(\frac{2r_0}{\Lambda_f}\right)^2 = \frac{1}{\pi^2} \cong 0.1$. Substituting Equation 14 or Equations 15 and 16 and 5 into Equation 7 we obtain

$$\dot{\varepsilon}_\theta = \frac{3\Gamma h}{2\tau_0 r^2}\dot{\varepsilon}_y \sinh\left(\frac{1}{2} + \pi\right) - \frac{\dot{\varepsilon}_y}{2}, \tag{17}$$

or

$$\dot{\varepsilon}_\theta = \frac{3\Gamma h}{2\tau_0 r^2}\dot{\varepsilon}_y \sinh\left[\frac{1}{2} + \pi - \left(\frac{2\Gamma}{3\tau_0 h}\right)\right] - \frac{\dot{\varepsilon}_y}{2}. \tag{18}$$

Substituting again the co-ordinate ξ using the relation

$$r = \xi - h/2 - r_0 = \xi - h/2 - (3\Gamma h/2\tau_0)^{1/2},$$

we obtain

$$\dot{\varepsilon}_\theta = \frac{3\Gamma h}{2\tau_0[\xi - h/2 - (3\Gamma h/2\tau_0)^{1/2}]^2}\dot{\varepsilon}_y \sinh\left(\frac{1}{2}+\pi\right) - \frac{\dot{\varepsilon}_y}{2}, \tag{19}$$

or

$$\dot{\varepsilon}_\theta = \frac{3\Gamma h}{2\tau_0[\xi - h/2 - (3\Gamma h/2\tau_0)^{1/2}]^2}\dot{\varepsilon}_y \sinh\left[\frac{1}{2}+\pi - \left(\frac{2\Gamma}{3\tau_0 h}\right)^{1/2}\right] - \frac{\dot{\varepsilon}_y}{2}. \tag{20}$$

Equations 19 and 20 approximate the component of the perturbed strain field ahead of the craze tip. It is seen from Equation 19 or Equation 20 that $\dot{\varepsilon}_\theta$ decreases with the distance from the craze tip and with decreasing craze tip opening h. The same picture emerges if instead of Equation 13 the current value of local stress from Equation 12 is substituted into either Equation 19 or Equation 20 as can be easily confirmed by numerical calculations.

Clearly, the distance from the craze tip, where the $\dot{\varepsilon}_\theta$ component of the perturbed field equals zero and thus matches the plane-strain conditions prevailing far ahead of the craze tip ($\dot{\varepsilon}_\theta = \dot{\varepsilon}_z = 0$), decreases with decreasing craze tip opening h.

It is a matter of interest to find the lowest critical value of the craze tip opening h_{crit} that still ensures that the perturbation will grow. As a criterion we take the condition that the perturbed field has to be confined within the zone of intensive plastic strains, i.e. within the exponential spiral slip line region, otherwise the relations described by Equations 12–15 do not hold. The lowest value of h_{crit} is reached just when the perturbed field matches the outer plane-strain field at $\xi = h_{crit}/2\exp\pi/2$. In Fig. 2 we have shown the normalised distance $\xi/(h/2)$ ahead of the craze tip as a function of h for different values of τ_0, where the $\dot{\varepsilon}_\theta$ component of the perturbed field matches the plane strain conditions. All curves are cut at points where the value of $\xi/(h/2)$ crosses the bound $\exp(\pi/2)$. It can be seen that as h increases the boundary of the perturbed field moves inside the exponential spiral slip line region. Thus h_{crit} can be expressed analytically from Equation 19 with $\dot{\varepsilon}_\theta(\xi = h_{crit}/2\exp\pi/2) = 0$ as

$$h_{crit} = \frac{6\Gamma}{\tau_0}\left\{\frac{[2\sinh(1/2+\pi)]^{1/2}+1}{\exp(\pi/2)-1}\right\}^2, \tag{21}$$

or, when using Equation 20, found by numerical solution of the transcendental equation

$$\left(\frac{3}{2}\right)^{1/2}\frac{\Gamma}{\tau_0}\sinh\left[\frac{1}{2}+\pi-\left(\frac{2\Gamma}{3h_{crit}\tau_0}\right)^{1/2}\right] = \frac{h_{crit}}{8}\left[\exp\left(\frac{\pi}{2}\right)-1-\left(\frac{6\Gamma}{\tau_0 h_{crit}}\right)^{1/2}\right]^2. \tag{22}$$

Having found the critical opening displacement h_{crit} we can estimate the upper and lower bounds for the fibril diameter $\bar{D}$ by the following simple geometric considerations. If we recall the starting assumption about the growth of corrugations being the combined increase of perturbation amplitude and the void "fingers" expansion, the picture of the final state of corrugation development may be drawn as shown in Fig. 3. The tip of void "finger" penetrates a distance $h_{crit}/2(\exp\pi/2 - 1)$ and touches the neighbouring void "finger" leaving behind tufts of material which will form the craze fibrils. The geometrical dimensions are indicated in Fig. 3. After the coalescence of the void "fingers", the tufts of material left in the wake, reshape to cylindrical form thereby reducing their surface energy. The lower bound of the fibril diameter is then identified with the radius of the circle that touches two neighbouring void finger circles and the z axis standing for the craze leading edge before the onset of perturbation. Thus

$$\bar{D}_{min} = \frac{[h_{crit}/2(\exp\pi/2-1) - \pi(3\Gamma h_{crit}/2\tau_0)^{1/2}]^2}{h_{crit}/2(\exp\pi/2-1)}. \tag{23}$$

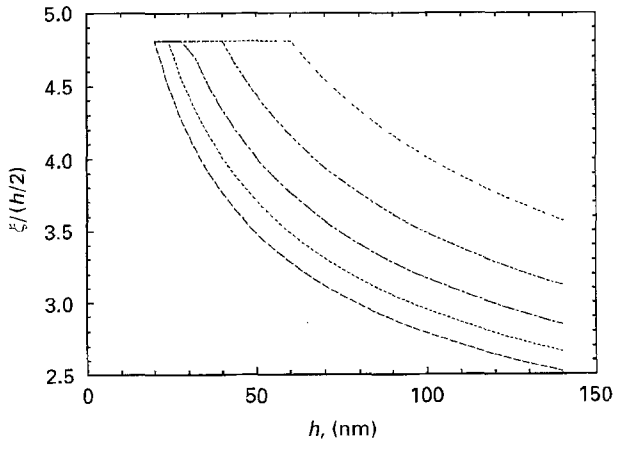

Figure 2 Plot of the normalised distance $\xi/(h/2)$ ahead of craze tip as a function of h for the values of τ_0 of:(--- ---) 10 MPa, (----) 15 MPa, (— —) 20 MPa, (— - —) 25 MPa and (— —) 30 MPa.

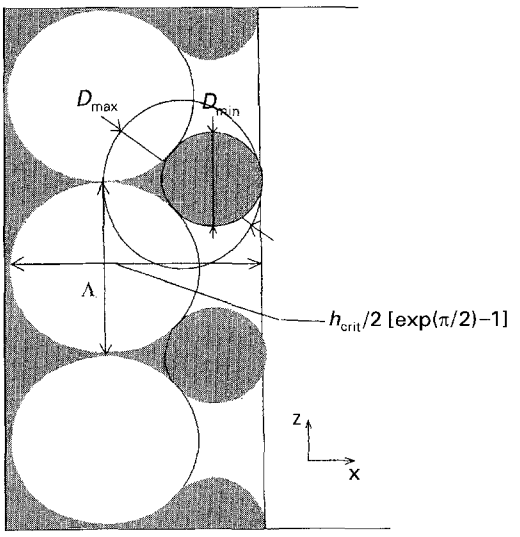

Figure 3 A geometrical construction for the fibril diameter $\bar{D}$ estimate.

The upper bound is taken as the diameter of the circle that touches the z axis and goes through the contact point of the void "fingers". This provides

$$\bar{D}_{max} = \frac{h_{crit}}{2}\left(\exp\frac{\pi}{2} - 1\right) - \pi\left(\frac{3\Gamma h_{crit}}{2\tau_0}\right)^{1/2} \quad (24)$$

and the fibril diameter $\bar{D}$ is assumed to be approximated by the geometrical mean of $\bar{D}_{max}$ and $\bar{D}_{min}$

$$\bar{D} = \left(\frac{[h_{crit}/2(\exp\pi/2 - 1) - \pi(3\Gamma h_{crit}/2\tau_0)^{1/2}]^3}{h_{crit}/2(\exp\pi/2 - 1)}\right)^{1/2}. \quad (25)$$

Finally, the relative volume of the craze fibrils v_f can be estimated as follows

$$v_f \cong \frac{\bar{D}^2}{\Lambda_f^2} = \frac{\tau_0 \bar{D}^2}{6\pi^2 \Gamma h_{crit}}. \quad (26)$$

Note that the value of $\bar{D}$ and v_f refer to the craze tip where the relative volume of craze fibrils and the mean fibril diameter are considerably smaller than the average values in the craze.

2.1.2. Numerical results and discussion

Equations 5 and 21–26 were evaluated for $\Gamma \in [0.02; 0.08]$ Jm^{-2} and $\tau_0 \in [10; 30]$ MPa. Whilst the chosen Γ values cover nearly the whole range of surface energies for many polymers, the chosen τ_0 range covers only a part of typical shear yield stress values of polymers. However, for our purposes it will be sufficient since the trends of the curves are quite apparent.

First let us examine the results obtained for h_{crit} via Equation 21, see Fig. 4. It is plausible that h_{crit} values lies within the interval [10–140] nm, since that is in accordance with experimental observations. The results obtained via Equation 22 which include the influence of the surface energy tension during the expansion of "fingers" are higher but differ by only 3–4%.

A somewhat greater influence of the correction in Equation 22 can be observed in the predicted values of fibril diameter where data obtained by using Equation 22 lie about 6% above the values computed when Equation 21 was used to estimate h_{crit}. As can be seen from Fig. 5, the predicted fibril diameter values vary from 8–100 nm, which is also consistent with experimental data for many polymers, especially at the lower end of the predicted range. The upper end of the predicted range was computed from combinations of the yield stress and surface energy values that do not usually occur in real polymers, i.e. low yield stress values and high surface energy values. This remark also holds for other parameters, i.e. h_{crit} and Λ_f.

The weakest influence of the correction in Equation 22 is encountered in the computation of the wavelength Λ_f, see Fig. 6, where the correction in Equation 22 provides values of Λ_f only about 1.5% higher. Λ_f can be identified with the mean spacing of fibrils and the results for Λ_f ranging from 20–260 nm are again quite realistic.

It is apparent from Figs. 4–6 that all the investigated parameters h_{crit}, $\bar{D}$ and Λ_f change remarkably with changes in the yield stress and surface energy. Using Equation 21, the analytical expressions for

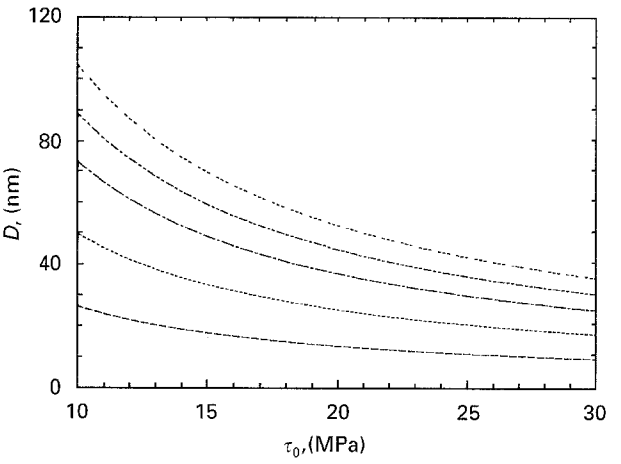

Figure 5 Plot of the fibril diameter $\bar{D}$ at the craze tip as a function of τ_0 for different values of Γ, h_{crit} computed after Equation 22. The values of Γ are those shown in Figure 4.

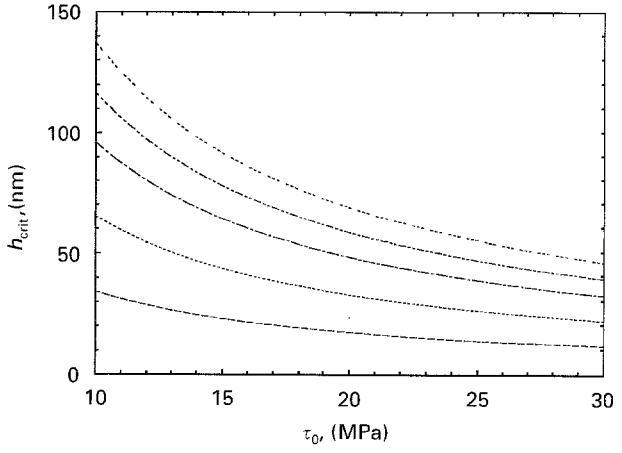

Figure 4 Plot of the critical displacement at the craze tip h_{crit} as a function of τ_0 for different values of Γ computed after Equation 21. The values of Γ are; (- - - -) 0.08 Jm^{-2}, (— — —) 0.068 Jm^{-2}, (— —) 0.056 Jm^{-2}, (— — —) 0.038 Jm^{-2}, and (— —) 0.02 Jm^{-2}.

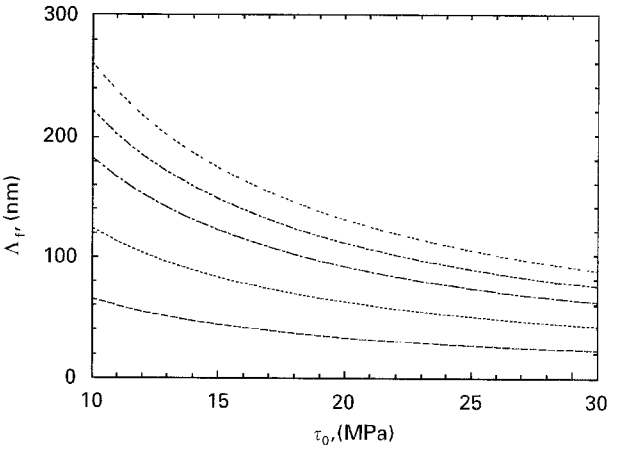

Figure 6 Plot of the wavelength Λ_f as a function of τ_0 for different values of Γ, h_{crit} computed after Equation 22. The values of Γ are those shown in Figure 4.

$\bar{D}$ and Λ_f are as follows;

$$\bar{D} = \frac{3\Gamma}{\tau_0} \frac{1}{\exp \pi/2 - 1} [A/(A - \pi)^3]^{1/2} \quad (27)$$

and

$$\Lambda_f = \frac{\pi A}{\exp \pi/2 - 1} \frac{6\Gamma}{\tau_0}, \quad (28)$$

where $A = [2\sinh(1/2 + \pi)]^{1/2} + 1 = 7.17$.
By inspection of $\bar{D}$ and Λ_f for different values of τ_0 and Γ, one can find that, due to a plasticizer, the microstructure of the craze could become coarser. This is especially the case with those polymers and environments where only a small change of the surface energy occurs. We will address the problem of the surface energy in more detail later.

A particular property of the model is that the relative fibril volume v_f computed from Equation 26 is constant for all combinations of τ_0 and Γ as can be easily seen from Equations 26–28. With h_{crit} computed via Equation 21 the volume fraction v_f is 0.14 and with h_{crit} computed via Equation 22 a value of 0.16 is obtained. Both values are in excellent agreement with the actual value of v_f at the craze tip which is reported for many polymers to be about 0.15–0.20. The prediction, that the fibrils volume fraction at the craze tip should be rather insensitive to changes in the yield stress and the surface energy, seems to be in accord, for example, with the findings of Brown and Njoku [19] for polystyrene (PS) plasticized between 0–20% of dibutyl phthalate (DBP). Only a slow change of the average fibril volume fraction with increasing content of DBP was reported. However, it has to be taken into account that, in air conditions, the vast majority of crazed matter is produced not at the craze tip, but further back by drawing from the substrate. With increasing content of plasticizer the mechanism of craze thickening starts to be replaced by fibril extension. Clearly this change in the craze thickening mechanism with increasing content of plasticizer may also be responsible for the slow change in fibril volume fraction and so the predicted insensitivity of fibril volume fraction at the craze tip to changes of yield stress and surface energy seems to be justified.

To discuss the influence of the surface energy change we start with the remark that some modification of the original entanglement network is necessary for the transition from randomly aligned entangled molecules to an array of oriented fibrils in the craze. In principle, Kramer [20] has noted that "geometrically necessary entanglement loss" could occur either by chain scission or by disentanglement of the chains thus allowing the transition to take place. In polymers such as PS, chain scission is the dominant mechanism of network modification under ambient conditions. The energy required to create the surface is then [21]

$$\Gamma = \gamma_w + \frac{1}{4}\eta d U, \quad (29)$$

where γ_w is the van der Waals surface energy, η is the density of network strands, d is the square root end-to-end distance between junction points in the network and U is the polymer backbone bond energy. The van der Waals surface energy for many polymers is about $0.04\ \mathrm{J\,m^{-2}}$. For a polymer with a strand density of $3 \times 10^{25}\ \mathrm{m^{-3}}$ the chain scission term approximately equals $0.04\ \mathrm{J\,m^{-2}}$ so that $\Gamma \approx 0.08\ \mathrm{J\,m^{-2}}$. Since ηd scales roughly as $\eta^{1/2}$, increasing the strand density of the network leads to a strong increase in Γ.

The effect of a plasticizer on Γ appears to consist of the promotion of a transition from scission-dominated crazing to disentanglement-dominated crazing due to enhanced chain slippage and a reduction of the van der Waals surface energy γ_w due to the interface polymer-environment. The former effect seems to be more important, especially when the crazing in air conditions is scission-dominated. The transition from scission-dominated crazing to disentanglement-dominated crazing as a function of temperature was explored by Berger *et al.* [22].

Thus, if the change in surface energy is primarily due to the transition from the scission-dominated to the disentanglement-dominated regime as a consequence of enhanced slippage and because the same mechanism of enhanced slippage controls the reduction of the yield stress it can be expected that within a certain range of temperature and/or plasticizer content the ratio Γ/τ_0 is constant. This results in a constant mean spacing of fibrils Λ_f, see Equation 28, which was actually observed by Berger *et al.* [22].

2.2. Thermodynamics of environmentally stimulated craze advance

Some initial ideas concerning the complex nature of ESC, developed from the viewpoint of irreversible thermodynamics, have been presented by Okamoto and Ohde [23]. An effective method for including the thermodynamics of crazes into a fracture mechanics approach has been sought by Chudnovsky *et al.* and Stojimirovic *et al.* [24, 25]. A detailed discussion of this work is beyond the scope of this review and we refer interested readers to the original papers.

2.2.1. Theoretical model

Consider a polymer sample with an isolated craze immersed in a certain kind of liquid and subjected to a deformation or load. Assume that the transport of liquid into the craze is assured either by side-flow, capillarity flow, following Darcy's flow law and/or diffusion. From a thermodynamic viewpoint, the state of the system consisting of the bulk material, a craze, an environment and a loading mechanism is, in general, unstable, since its thermodynamic potential is not at a minimum. For further development it is desirable to specify the term "thermodynamically unstable". In fact, in the problem with which we are dealing, the thermodynamic nonequilibrium is created by two sources. One is the intrinsic metastable state of glassy polymer, which is more or less far from thermodynamic equilibrium. The other is the system including the environment and the polymer which tends towards the equilibrium state according to the laws of thermodynamics of mixtures and strongly affects the

mechanical stability of the crazed sample and the loading mechanism. The former can be described within the framework of rational thermodynamics, see for example the work of Kestin and Rice [26] who used the concept of internal variables to characterize the microstructural pattern of the material. For its application to polymers see for example the work of Struik [27]. The formalism of equilibrium thermodynamics is then adopted for processes which are running far from equilibrium through a sequence of so-called constrained equilibrium states. The processes are understood to be reversible if no changes in the values of internal variables occur. This concerns the bulk of the polymer which will be characterized as an elastic body. In other words, it is implicitly considered that the relaxation times of physical aging in a bulk polymer are much longer than the relaxation times characterizing the transition towards equilibrium between the polymer in craze zone and environment. It is also assumed that the applied load is relatively small with respect to the yield stress of the polymer. The whole system is schematically depicted in Fig. 7.

As indicated in Fig. 7, only isothermal processes are investigated. The environment may be assumed as a reservoir with its intensive parameters remaining constant. There is no exchange of energy or particles between the environment and the bulk material. The restriction for no exchange of particles between the craze zone and the bulk may seem to be too restrictive. In reality, some diffusion of small liquid molecules into the surrounding bulk can take place and, due to plasticization, it can support the drawing of new fibril material into the craze. However, the mechanical interaction between the bulk material and craze zone is of primary importance. As far as the bulk is concerned, only the total elastic strain energy and the potential energy of the loading mechanism may change during the process of liquid transport into the craze.

For the system consisting of environmental liquid and polymeric material and under the assumption that no polymer molecules are in the liquid, the Helmholtz free energy is

$$F = n_r \mu_r + n_{s,1} \mu_{s,1} - p_1 V_1 + n_{s,2} \mu_{s,2} - p_2 V_2, \quad (30)$$

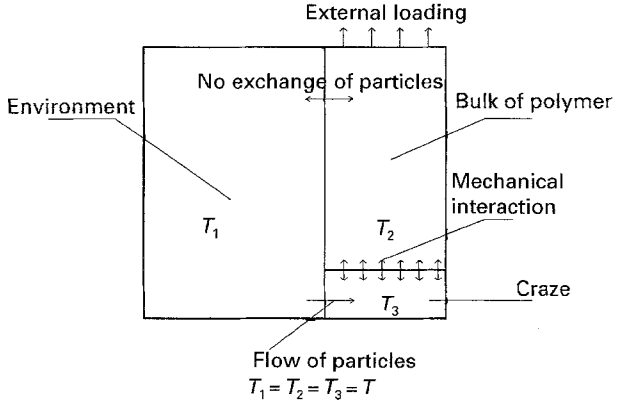

Figure 7 The scheme of the thermodynamic interaction between the crazed polymer and the environment.

where μ_r and $\mu_{s,1}$ are the chemical potentials of a polymer molecule and a liquid molecule respectively in phase 1 (taken to be the polymeric material) and $\mu_{s,2}$ is the chemical potential in phase 2 (taken to be the liquid environment).

The nonequilibrium condition between the phases implies that irreversible spontaneous processes take place. The Helmholtz free energy of the whole system decreases reaching a minimum value in the equilibrium state. It is clear from Equation 30 that the decrease in Helmholtz free energy of the environment is caused by the removal of some liquid molecules since, as stated above, the intensive properties are assumed to be constant in the environment. Thus, it seems obvious to attribute the main change in the Helmholtz free energy to the part corresponding to the polymeric material.

The Helmholtz free energy change of the polymeric material in the craze is suitably approximated by the Flory–Huggins lattice theory [28]. The corresponding density of the Helmholtz free energy change (i.e. related to the unit volume of mixture of polymer and liquid in craze fibrils) is then

$$\Delta f_M = \frac{RT}{V^r_{m2}} \times$$

$$\left\{ \frac{\varphi}{s} \ln\varphi + \frac{1-\varphi}{r} \ln(1-\varphi) + \frac{1}{s}\chi(1-\varphi)\varphi + \frac{\rho V^s_{m1}}{M_c} \right.$$

$$\left. [(1-\varphi)^{1/3} - (1-\varphi)/2] - \frac{\Delta p V^s_{m1}}{RT}\varphi \right\}, \quad (31)$$

where φ denotes the average concentration of liquid in the craze fibrils, R denotes the gas constant, T is the absolute temperature, V^r_{m2} is the molar volume of a segment of polymer molecules and V^s_{ml} is the molar volume of a segment of liquid molecules. The Flory–Huggins relation takes into account various factors. First, the entropy of mixing is considered in the first two terms on the right side of Equation 31 with r standing for the number of elements of polymer molecules and s standing for the number of elements of liquid molecules. Secondly, the energy of mixing is taken into account by the third term with χ standing for the polymer–liquid interaction parameter. The fourth term on the right side concerns the elastic energy changes on swelling, with ρ being the density of polymer and M_c the molecular weight of a network chain molecule. The last term in Equation 31 expresses the influence of dilatant stress on swelling which is very important under higher stress levels and incompatible liquids with higher values of χ. $\Delta p = p_1 - p_2$, p_1 being the ambient pressure and $p_2 = -\sigma_Y/3$, where p_2 is the negative pressure in the fibrils due to an uniaxial true loading stress σ_Y which can be identified with the yield stress in simple tension. If the ambient pressure p_1 is atmospheric pressure, it can be neglected. Note that the yield stress is generally reduced due to plasticization and depends on the concentration φ of the liquid in craze fibrils. The approximation from Equations 1 and 2 will be used for σ_Y in Equation 31.

The semi-cohesive zone model will be used to model the whole craze zone. This model is usually understood to be a modification of the Dugdale–Barenblatt model which includes two distinctive non-linear zones at the crack tip. The zone immediately next to the crack is semi-cohesive in that it is filled with microcracks and voids whilst the further cohesive zone is a standard plastic zone. For the application of this model to an isolated craze in a glassy polymer let us first consider the schematic diagram of the cross-section of a full craze shown in Fig. 8. The main body of the craze has a sensible constant thickness which may vary from somewhat less than 1 μm to several μm depending on the polymer and the temperature. Over a distance of some tens of μm the thickness of the craze decreases to a crack-like tip, reminiscent in shape of the Dugdale plastic zone although, as shown in the paper of Lauterwasser and Kramer [29], the stress over the tip region is not a constant. Further, it was argued convincingly by Argon *et al.* [30] that if the craze is not to show accelerated growth rates, the stress along the body of the craze must approach the applied stress at a distance far from the craze tip region, i.e. along the main part where the craze no longer thickens. We will call this part the inert zone. Schematically, three different zones can be distinguished along the craze length:

(1) the plastic zone (a–b) at the craze tip, where the convolution by Taylor meniscus instability operates.

(2) the active zone (b–c), where the craze thickening mainly by drawing of new material from craze flanks takes place,

and

(3) the inert zone $2c$, where the craze no longer thickens.

To make further analysis as tractable as possible, the stress along each of these zones is considered to be a constant having different values within each zone. Thus in fact, the 2-zone model of craze introduced by Verheulpen-Heymans and Bauwens [31] is extended to the 3-zone model.

Such a combination of zones matches the physical mechanism of craze growth by Taylor meniscus instability and approximates to the stress distribution in the region of craze tip.

The equilibrium of inert/active/plastic zones shown in Fig. 8 is expressed in terms of a modified Barenblatt model as

$$K[\sigma_\infty] + K[\sigma_{0c}] + K[\sigma_c] + K[\sigma_Y] = 0, \quad (32)$$

where the elastic stress intensity term $K[\sigma_\infty]$ corresponds to the full craze length a, the semi-cohesive term $K[\sigma_{0c}]$ corresponds to the inert zone contribution, the semi-cohesive term $K[\sigma_c]$ to the active zone contribution and the cohesive term $K[\sigma_Y]$ to the plastic zone contribution. According to Eshelby [32], Equation 32 can be written in the form

$$\pi\sigma_\infty - 2(\sigma_Y - \sigma_c)\cos^{-1}b/a - 2\sigma_c\cos^{-1}c/a - 2\sigma_{0c}\sin^{-1}c/a = 0, \quad (33)$$

where σ_∞ is the remote applied stress, σ_{0c} is the stress within the inert zone of craze, σ_c is the stress along the active zone and σ_Y is the yield stress within the plastic zone.

Note that the model includes a threshold applied stress intensity, and thus a plastic zone, below which a craze will not grow. Above this, a craze will begin to grow with an individual plastic zone larger than the threshold value. As the craze becomes longer, the fibrils within the craze pull back on the opening surfaces gradually reducing the stress intensity at the craze tip. Finally, at equilibrium the plastic zone at the craze tip has returned to the threshold value. The determination of the opening displacement over the particular zones is slightly more complex and is shown in Appendix 1.

The equilibrium condition of Equation 33 is not solely sufficient to determine the length of a particular zone. Some extra criterion has to be included to resolve this problem. For example, the threshold length of the plastic zone can be determined using the expression for the opening displacement in (A6) and putting it equal to the critical opening displacement derived in the preceding section, see Equation 21.

A mixed thermodynamic–fracture mechanics approach to the craze advance begins by specifying the global change of the Gibbs potential of the polymer and the loading mechanism as a consequence of the possible migration of the interface, $\partial\mathbf{V}_{craze}$, between the bulk and the craze and also the translation of active zone/plastic zone in the direction of craze advance. It can be conveniently expressed in terms of Eshelby's tensor, i.e. energy momentum tensor of the elasticity $\boldsymbol{P}$ [33]

$$\delta G = -\int_{\partial V_{craze}} \delta\xi_i [P_{ij}] n_j \mathrm{d}\Xi, \quad (34)$$

where $\delta\xi_i$ is a virtual displacement vector at each point of ∂V_{craze}, describing the migration of the interface, $njd\Xi$ is an oriented surface element and $[P_{ij}]$ is the jump across the interface of the Eshelby tensor component, P_{ij}

$$P_{ij} = f\delta_{ij} - \sigma_{ki}u_{k,j}. \quad (35)$$

In Equation 35 f stands for the Helmholtz free energy density in the case of isothermal change, δ_{ij} is the Kronecker symbol, σ_{kj} are the Cauchy stress tensor components, u_k denotes the displacement vector components and $u_{kj} = \partial u_k/\partial x_j$ is a deformation gradient.

To render the problem more tractable we assume that the active/plastic zones are planar zones, i.e. their width, $y(x_1)$, is significantly smaller than their total length a-c. Neglecting the terms of the order $y/(a\text{-}c)$ (since $y/(a\text{-}c) \ll 1$), the normal vector of the bulk/craze

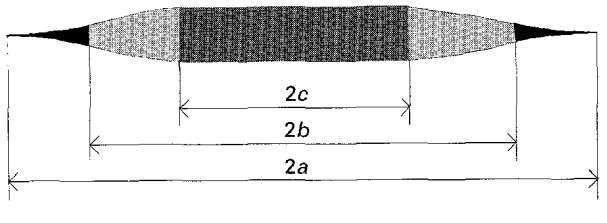

Figure 8 Schematic diagram of the cross section of a craze.

boundary $\boldsymbol{n}$ can be approximated by $\boldsymbol{n} = (0, 1)$ everywhere except at the very tip of the plastic zone. The first component of the vector $\delta\xi_i$ is chosen as a virtual increase of the craze length δa. The second component is normal to the bulk/zones interface and it will be specified later. Equation 34 can then be recast in the following form

$$\delta G = -\int_{\partial V_{ca}} \delta\xi_2 (P^B_{22} - P^Z_{22}) dx_1 - \delta a$$

$$\times \int_{\partial V_{ca}} (P^Z_{12} - P^C_{12}) dx_1 - \delta a \lim_{\varepsilon \to 0} \int_{\partial V_\varepsilon} P^B_{1j} n_j dG . \quad (36)$$

In Equation 36 the superscript 'B' refers to quantities related to the bulk material, whereas the material of the craze is labelled with the superscript 'Z'. ∂V_{ca} denotes the planar interface between the zones and the bulk on the upper and lower active/plastic zones surfaces. The first term on the right-hand side of Equation 36 corresponds to the change in the Gibbs potential, G, due to the expansion of the active/plastic zones. The integration over the inert zone is not included in this term because, as stated above, the inert zone no longer becomes thicker. The second term corresponds to the change of the Gibbs potential due to the translation of both zones. Note that the brackets in Equation 34 were defined in the second term of Equation 36 in a slightly different way – namely, due to the translation of zones in the direction of craze advance, the interface ∂V_{ca} gradually becomes a part of the inert zone/bulk interface where the Eshelby tensor component P^C_{12} has to be applied. However, it holds by definition that $u_{2,1} = 0$ along the inert zone, which in view of Equation 35 gives $P^C_{12} \equiv 0$ and the integral in the second term turns into the well known J-integral of fracture mechanics. The third term in Equation 36 represents the change in the Gibbs potential due to the shift of the tip of the plastic zone. ∂V_ε is a contour encompassing the plastic zone tip. The integration of this term is readily performed by means of the asymptotic solution [34]

$$\lim_{\varepsilon \to 0} \int_{\partial V_\varepsilon} P^B_{1j} n_j d\Gamma = \frac{K^2_{tip}}{E}, \quad (37)$$

where K_{tip} is the stress intensity factor characterizing the elastic field in the vicinity of the plastic zone tip, and E is the Youngs modulus of the polymer. Note that for plane strain condition the Youngs modulus E has to be replaced by $E/(1 - \nu^2)$ everywhere in the text with ν standing for the Poisson's ratio. Note also that P^Z_{1j} gives no contribution to the integral (having weaker elastic field singularity than P^B_{1j}).

The integral in the second term becomes

$$J = \int_{\partial V_{ca}} P^Z_{12} dx_1 = -\int_c^a \sigma_{22} \left(\frac{\partial u_2^+}{\partial x_1} - \frac{\partial u_2^-}{\partial x_1} \right) dx_1$$

$$= -\int_c^a \sigma_{22} \frac{\partial y}{\partial x_1} dx_1 , \quad (38)$$

where $u_2^+ - u_2^+ = y$ is the opening displacement in the zones. With reference to the 3-zone model described above, the last right-hand side integral yields

$$-\int_c^a \sigma_{22} \frac{\partial y}{\partial x_1} dx_1 = \sigma_c [y(c) - y(b)] + \sigma_Y y(b) , \quad (39)$$

where $y(c)$, and $y(b)$ are the displacement openings at the inert zone tip and at the active zone tip respectively, (see Appendix 1).

Let us first assume that $P^B_{22} = P^Z_{22}$. Then Equation 36 reduces to

$$-\frac{\partial G}{\delta a} = \sigma_c [y(c) - y(b)] + \sigma_Y y(b) + \frac{K^2_{tip}}{E}, \quad (40)$$

or, under the assumption of small scale yielding and by the definition of Irwin's potential energy release rate, $-\partial G/\partial a = K^2/E$

$$\frac{K^2}{E} = \sigma_c [y(c) - y(b)] + \sigma_Y y(b) + \frac{K^2_{tip}}{E}, \quad (41)$$

where K is the applied stress intensity factor. Because the extent of all zones along the craze is determined by the condition that the stresses are to be non-singular, $K_{tip} = 0$ and one can easily recognize that Equation 41 reduces to the well known relation in fracture mechanics $-\partial G/\partial a = J$.

We now consider the general case when the jump of the normal component P_{22} of Eshelby's tensor in the first right-hand side term of Equation 36 reaches a value γ.

$$\gamma = P^B_{22} - P^Z_{22}. \quad (42)$$

It follows from the definition of Eshelby's tensor Equation 35 that the specific energy γ is comprised of the differences between the Helmholtz free energy densities and also the work densities of the material before and after the transition from the dry bulk to the craze fibrils with absorbed environment liquid. In the following we will approximate the specific energy, γ, by the free energy density change introduced in Equation 31. However, because in our definition the change of the free energy density is defined as the difference between the final and the initial state of system we write

$$\gamma \cong -\Delta f_M . \quad (43)$$

It is postulated that this change of free energy occurs only across the interface between the bulk and the active craze zone. Further, the virtual displacement, $\delta\xi_2$, is chosen as half of the virtual craze thickening, $\delta t(x_1)$. $t(x_1)$ is related to the draw ratio, λ, and the craze displacement, $y(x_1)$, by

$$t(x_1) = \frac{\lambda}{\lambda - 1} y(x_1), \quad (44)$$

see Appendix 2. Under the assumption of constant draw ratio along the active craze zone the virtual craze thickening $\delta t(x_1)$ is

$$\delta t(x_1) = \frac{\lambda}{\lambda - 1} \delta y(x_1)$$

and the first term on the right-hand side of Equation 36 becomes

$$-\int_{\partial V_{ca}} \delta\xi_2(P_{22}^{B} - P_{22}^{Z})\mathrm{d}x_1 = -\int_{\partial V_{cb}} \delta\xi_2(P_{22}^{B} - P_{22}^{Z})\mathrm{d}x_1$$

$$= \Delta f_M \frac{\lambda}{\lambda - 1}\int_c^b \delta y(x_1)\mathrm{d}x_1, \quad (45)$$

where Δf_M is approximately considered to be a constant along the active zone and is put outside the integral. The craze displacement opening y can be generally described by the function $y = y(x_1, a, b, c)$ (see Appendix 1), so that the virtual displacement δy related to the virtual advance of craze length δa reads

$$\delta y(x_1) = \left|\frac{\partial y(x_1, a, b, c)}{\partial a}\right|_{\substack{b=\text{const}\\ c=\text{const}}} \delta a\,. \quad (46)$$

Substituting Equation 46 into Equation 45 and applying the result of Rice [35] (see Appendix 3) to the right side term we get

$$\Delta f_M \frac{\lambda}{\lambda - 1}\int_c^b \frac{\partial y(x_1, a)}{\partial a}\mathrm{d}x_1 = \Delta f_M \frac{\lambda}{\lambda - 1}\frac{2K'K[\sigma_c]}{E\sigma_c}, \quad (47)$$

where the external stress intensity factor, K', generally differs from K in Equation 41. Combining Equations 47, 45, 39, 37 and 36 and assuming that $K_{tip} = 0$ in Equation 37 we finally arrive at

$$\frac{K'^2}{E} = -\frac{2\Delta f_M}{E}\frac{\lambda}{\lambda - 1}\frac{K'K[\sigma_c]}{\sigma_c} + \sigma_c[y(c) - y(b)] + \sigma_Y y(b)\,. \quad (48)$$

Consider for a moment that the distribution of zones along the craze and their opening displacements are the same as in Equation 41 (with $K_{tip} = 0$). Then Equation 41 can be substituted into Equation 48 leading to

$$K'^2 = -2\Delta f_M \frac{\lambda}{\lambda - 1}\frac{K'K[\sigma_c]}{\sigma_c} + K^2\,. \quad (49)$$

Since $\Delta f_M < 0$ and $K[\sigma_c] < 0$, it follows from Equation 49 that generally $K' < K$. Solving Equation 49 for the ratio K'/K we obtain

$$\frac{K'}{K} = -\Delta f_M \frac{\lambda}{K(\lambda - 1)}\frac{K[\sigma_c]}{\sigma_c} + \left[\left(\Delta f_M \frac{\lambda}{K(\lambda - 1)}\frac{K[\sigma_c]}{\sigma_c}\right)^2 + 1\right]^{1/2}. \quad (50)$$

Equation 50 provides the reduction of the external stress intensity factor (or more simply, external load if the total length of craze, a, is a constant). Thus, the same craze thickness and zones distribution as for a craze in air conditions is reached with a lower external load, due to the additional driving force which is provided by thermodynamic instability between the craze material and environment. This effect is superimposed over the effect of environment on the material properties related to the crazing as investigated in the preceding section.

2.2.2. Numerical results and discussion

The expression on the right-side of Equation 31 was evaluated as a function of φ in the range $\varphi \in 0$–0.6 with the parameters having the following values: $T = 300$ K, $M_c \in 50\,000$–$500\,000$, $\rho = 10^3$ kg m^{-3}, $\chi \in 0$–0.35, $r \in 10^3$–10^4, $s = 8$, $\Delta p = \sigma_Y/3$, $\sigma_Y \in 8.5$–52 MPa, and under the assumption $V^{r}_{m2} \approx V^{s}_{m1}$. Correction was made to take account of the liquid concentration on yield stress according to Equation 2. The results in Fig. 9 were computed with a value of the interaction parameter $\chi = 0.25$ and molecular mass $M_c = 50\,000$. One can see that the minimum of the Helmholtz free energy density is reached for a concentration φ of about 0.27. The strong influence of the value of σ_Y is quite apparent. The same computation made with $M_c = 500\,000$ did not reveal any marked differences.

The results in Fig. 10 were obtained for $\sigma_Y = 52$ MPa and they demonstrate a rather weak influence of χ on Δf_M in comparison with the influence of σ_Y. When the correction for the effect of liquid concentration on the yield stress in omitted, the Helmoltz free energy decreases monotonously for $\sigma_Y \geq 10$ MPa as displayed in Fig. 11. Obviously, the

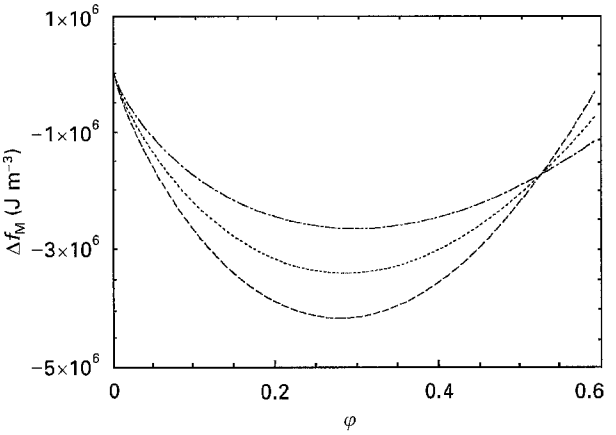

Figure 9 Plot of the Helmholtz energy density Δf_M as a function of φ for $\chi = 0.25$ and values of σ_Y of (– – –) 17 MPa, (– – – –) 35 MPa and (———) 52 MPa.

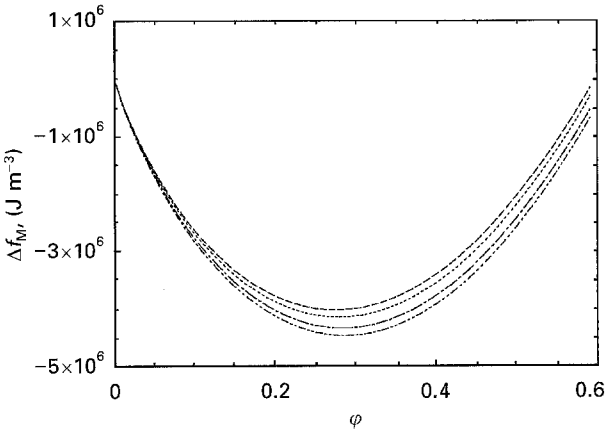

Figure 10 Plot of the Helmholtz energy density Δf_M as a function of φ for $\sigma_Y = 52$ MPa and values of χ of; (– – –) 0.35, (– – – –) 0.25, (———) 0.1 and (— — —) 0.

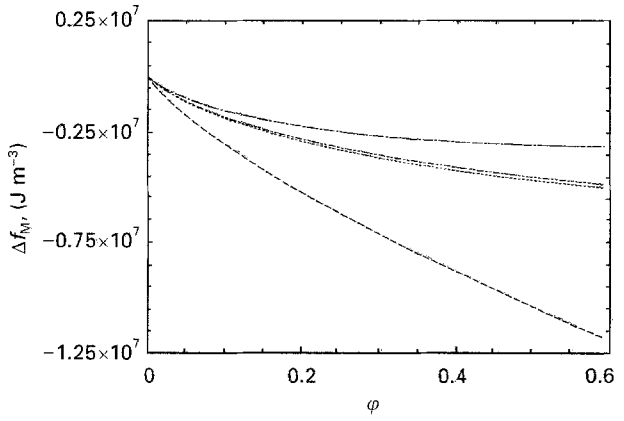

Figure 11 Plot of the Helmholtz energy density Δf_M as a function of φ with $\chi = 0.25$ without the correction to Equation 2. The values of σ_Y used were; (– – —) 8 MPa, (– – – –) 17 MPa and this case $\chi = 0.35$, (– – – –) 17 MPa and (– – –) 52 MPa.

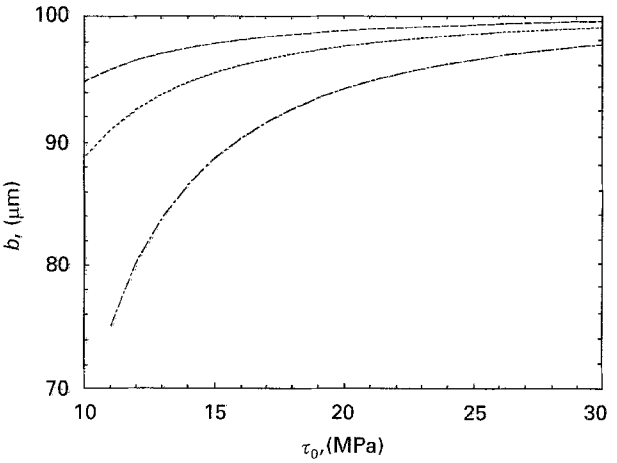

Figure 12 Plot of the total half-length of inert and active zone b as a function of τ_0 for various values of total surface energy Γ fulfilling the condition of critical displacement opening of Equation 26. The values of Γ used were; (– – –) 0.02 Jm^{-2}, (– – – –) 0.038 Jm^{-2} and (– – – –) 0.08 Jm^{-2}.

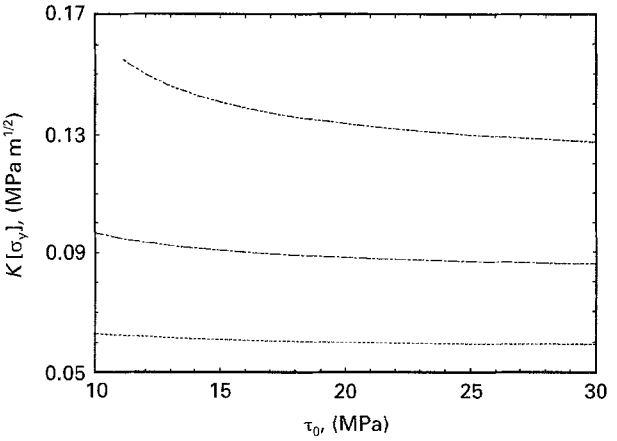

Figure 13 Plot of the absolute value of the critical stress intensity factor of plastic zone as a function of τ_0 for values of Γ of (– – – –) 0.08 Jm^{-2}, (– – –) 0.038 Jm^{-2} and (– – – –) 0.02 Jm^{-2}.

conclusion can be easily drawn that the last term in Equation 31 is dominant.

As follows from Figs 9 and 10, the minimum value of Δf_M is about $3 \times 10^6 - 4 \times 10^6$ J m^{-3} and this value will be used in subsequent computations.

To evaluate the ratio K'/K in Equation 50 one first has to generate a set of cohesive K-factor values $K[\sigma_{0c}]$, $K[\sigma_c]$, $K[\sigma_Y]$ which fulfil the equilibrium condition of Equation 32 or, equivalently, a set of lengths b and c fulfilling Equation 33, and which comply with certain criteria. The first criterion which is required to be met is the critical opening displacement at the base of the craze plastic zone since the aim is to investigate the state of initiation of the craze advance. Equation 21 from the first section and Equation A6 from Appendix 1 provide the following equation

$$21.3\frac{\Gamma}{\tau_0} = \frac{8}{\pi E}(\sigma_Y - \sigma_c) b \ln\frac{a}{b}, \qquad (51)$$

where $\sigma_Y = 3^{1/2}\tau_0$, $\sigma_c \cong \frac{2\times 10^3}{3}\left[\frac{\Gamma\tau_0}{5\times(3)^{1/2}}\right]^{1/2}$ [36],

and the length a of the craze has been chosen to be 100 μm. Equation 51 was solved for b with different values of τ_0 and Γ. The plots of b as a function of τ_0 are shown in Fig. 12. Note, that the plot of $b(\tau_0)$ for $\Gamma = 0.08$ J m^{-2} is not displayed over the whole range of τ_0 values because a solution was not found at the lowest values of τ_0. The cohesive stress intensity factor of the plastic zone $K[\sigma_Y]$ was computed for corresponding values of b from the standard formula

$$K[\sigma_Y] = 2\sigma_Y\left(\frac{a}{\pi}\right)^{1/2}\cos^{-1}(b/a) \qquad (52)$$

and its absolute value is plotted as a function of τ_0 for various values of Γ in Fig. 13. Since $K[\sigma_Y]$ stands for a certain threshold applied stress intensity below which the craze advance cannot be initiated (see also the text below Equation 33), it is interesting to note that if an environment does not affect the total surface energy Γ, the threshold applied stress intensity even slightly grows due to plastification.

The results obtained by solving Equation 51 were employed as an input data set for computer generation of a series of half-length c (see Fig. 14). The unknown value of the stress along the inert zone, σ_{0c}, was taken as a variable, and the values of b, τ_0 and σ_{0c} were entered as parameters for each particular series. The surface energy Γ was taken as a constant for all computations and equalled 0.038 J m^{-2}, and the external remote stress σ_∞ was set at 9 MPa. All those generated curves $c(\sigma_{0c})$ which did not comply with the experimentally justified condition

$$y(c) \geq 2y(b), \qquad (53)$$

where $y(c)$ is given by Equation A8 and $y(b)$ by Equation 51, have been automatically excluded. The plots in Figs 14 and 15 show some of the generated data sets of c values as a function of non-dimensional normalized stress $\sigma_{0c}/\sigma_\infty$ for various values of σ_c within the active zone and, correspondingly, for various values of σ_Y within the plastic zone of the craze. The sets of c values are also displayed only over the intervals where the solution of Equation 33, 51 and 53 was found. Note that the admissible values of the normalized variable $\sigma_{0c}/\sigma_\infty$ lie within the interval 0.67–0.8. Since the actual value of σ_{0c} is not known,

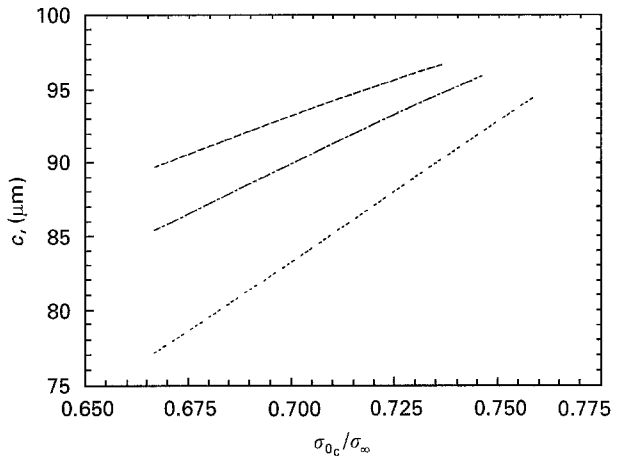

Figure 14 Plot of computer generated sets of the half-length c of the inert zone as a function of normalized stress $\sigma_{0c}/\sigma_\infty$ for values of σ_c of (– – –) 1.13 with $b = 98.9$ μm, (– – –) 1.06 with $b = 98.7$ μm and (– – – – – –) 0.99 with $b = 98.4$ μm.

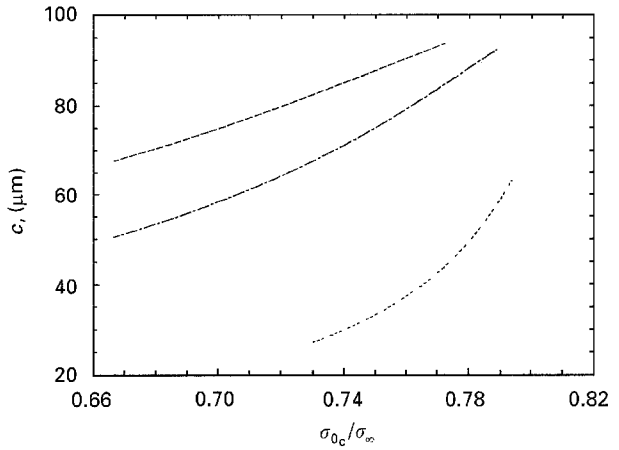

Figure 15 Plot of computer generated sets of the half-length c of the inert zone as a function of normalized stress $\sigma_{0c}/\sigma_\infty$ for the values of σ_c/σ_∞ of (– – –) 0.94 with $b = 98.0$ μm, (– – –) 0.89 with $b = 97.6$ μm and (– – – – – –) 0.84 with $b = 97$ μm.

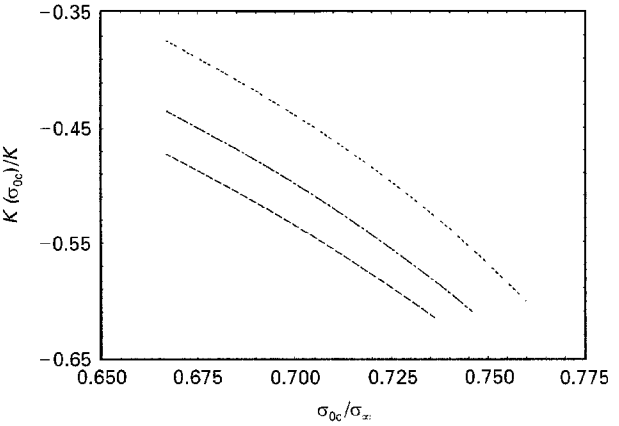

Figure 16 Plot of computer generated sets of normalized cohesive stress intensity factor of the inert zone as a function of normalized stress $\sigma_{0c}/\sigma_\infty$ for various values of σ_c/σ_∞ of (– – – – – –) 0.99 with $K[\sigma_c]/K = -0.09$ (– – –) 1.06 with $K[\sigma_c]/K = -0.085$ and (– – –) 1.13 with $K[\sigma_c]/K = -0.083$.

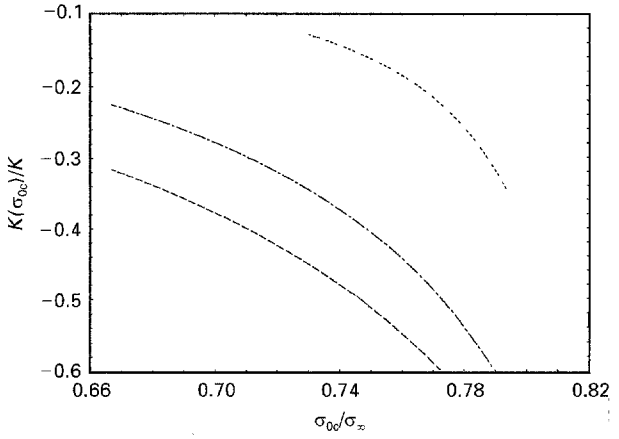

Figure 17 Plot of computer generated sets of normalized cohesive stress intensity factor of the inert zone as a function of normalized stress $\sigma_{0c}/\sigma_\infty$ for various values of σ_c/σ_∞ of (– – – – – –) 0.84 with $K[\sigma_c]/K = -0.34$, (– – –) 0.89 with $K[\sigma_c]/K = -0.096$ and (– – –) 0.94 with $K[\sigma_c]/K = -0.094$.

the only thing which can be done is to further eliminate those sets which are not apparently in accord with experimental observations. By inspection of Figs 14 and 15, this concerns particularly the lower set of generated data in Fig. 15 (the curve generated for $\sigma_c/\sigma_\infty = 0.84$) since the predicted values of c are too short and the upper set in Fig. 14 ($\sigma_c/\sigma_\infty = 1.13$) where, conversely, the predicted values of the half length of the inert zone c are too long for the given total craze length a and create 95% of the total craze length. It is interesting to see the corresponding values of the cohesive K-factor $K[\sigma_{0c}]$ which are plotted as non-dimensional normalized values $K[\sigma_{0c}]/K$ against $\sigma_{0c}/\sigma_\infty$. in Figs 16 and 17. Notice in the legend of Figs 16 and 17 that the cohesive K-factor of the active zone increases with decreasing stress σ_c acting over this zone. This occurs because of a simultaneous, more dominant increase of the active zone length $b-c$ as follows from Figs 14 and 15. Finally, we can discuss the main goal of this paper, namely the reduction of external load for the initiation of a craze advance due to the thermodynamic instability between the craze material and environment as predicted by Equation 50. Employing the preceding results, Equation 50 has been plotted as a function of normalized stress $\sigma_{0c}/\sigma_\infty$. The same combination of the other parameters has been used as indicated in the legends of Figs 18 and 19. If, as with the data sets for c values, the upper set in Fig. 18 and the lower set in Fig. 19 are excluded, it is possible to state the predicted reduction of external stress intensity factor, or external load for constant craze length, lies in the range 0.75–0.94. This means that the craze advance in an environment can occur under a lower external stress level than in air even if the material properties of the polymer are not affected. The traditional approach for explaining why glassy polymers are more prone to undergo crazing in some environments is based on experimental and theoretical evidence of plasticization which leads to a drop in the stress needed for crazing. This is generally accepted, especially for propagating crazes. However, some difficulties arise concerning the explanation for a lower threshold load level for the initiation of craze advance especially in cases when the environment affects the surface energy only slightly or not at all. Fig. 13 then shows clearly that the threshold

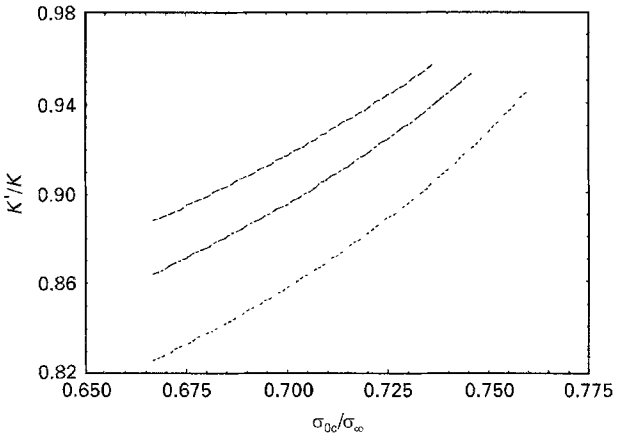

Figure 18 Plot of the reduction of external stress intensity factor as a function of normalized stress $\sigma_{0c}/\sigma_\infty$ for values of σ_c/σ_∞ of; (– – –) 1.13, (– · –) 1.06 and (– – · –) 0.99.

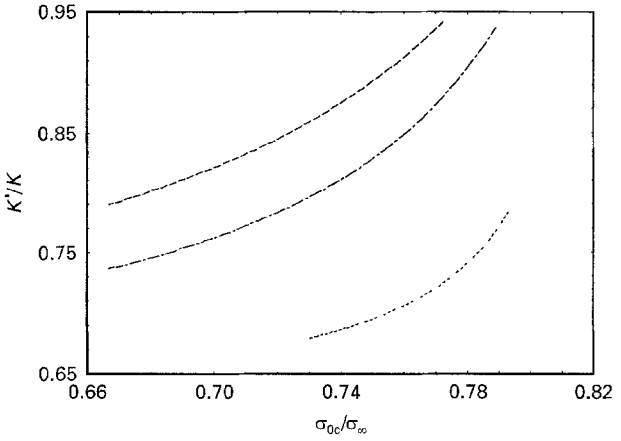

Figure 19 Plot of the reduction of external stress intensity factor as a function of normalised stress $\sigma_{0c}/\sigma_\infty$ for values of σ_c/σ_∞ of; (– – –) 0.94, (– · –) 0.89 and (– – · –) 0.84.

applied stress intensity even increases with decreasing yield stress. The model proposed in this paper can solve this problem since it predicts a higher applied local stress intensity in the craze tip due to the environment.

3. Conclusions

Micromechanical analysis of the initiation of craze advance provides the geometrical characteristics of craze microstructure as the mean fibril spacing, mean fibril diameter, the volume fraction of fibrils and critical opening displacement at the craze tip and relates them to basic material parameters such as yield stress and surface energy. The derived expression for the critical displacement at the craze tip h_{crit} could be used in the criterion for the initiation of craze advance

$$h \geq h_{crit} = 21.3\frac{\Gamma}{\tau_0}. \tag{54}$$

Remembering the known effect of plasticizers on the yield stress and the surface energy the influence of plasticizers on the craze microstructure is then discussed.

Starting with the idea of the thermodynamic non-equilibrium between the polymer at the craze tip region and its environmental liquid, the thermodynamic potential is constructed in terms of irreversible thermodynamics as a function of the concentration of liquid absorbed in the craze and dilatant stress in fibrils. Some simplifying assumptions are necessary to make the problem tractable. The spontaneous decrease of the thermodynamic potential provides an additional driving force for craze growth. The key problem for including this force in the fracture mechanics framework is overcome by using the Eshelby tensor [33]. Detailed analysis provides us with an expression for the effective reduction of applied stress intensity factor which is required for the initiation of craze advance. The investigated phenomenon shows that an ESC agent can provide a certain kind of antishielding of craze tip and thus increase the liability to craze growth. Numerical calculations demonstrate the various features of the model proposed.

Acknowledgements

The author wishes to thank the Royal Society of London for its generous financial support and the Department of Materials Engineering, University of Swansea for making this work possible.

Appendix 1

Following the Bilby, Cottrell and Swinden approach of representing the plastic zone by a distribution of dislocations, the equilibrium of each dislocation requires that

$$\frac{Eb'}{4}\int_{-a}^{a}\frac{f(x_1)}{x_1 - x_1'}\,dx_1 = g(x_1), \tag{A1}$$

where

$$g(x_1) = \sigma_\infty - \sigma_{0c} \quad \text{for } |x_1| < c$$

$$g(x_1) = \sigma_\infty - \sigma_c \quad \text{for } c < |x_1| < b$$

$$g(x_1) = \sigma_\infty - \sigma_Y \quad \text{for } b < |x_1| < a$$

and b' is the Burgers vector of dislocations, and $f(x_1)$ represents the number of dislocations between x_1 and $x_1 + dx_1$.

The solution to Equation A1 is

$$f(x_1) = -\frac{4(x_1^2 - a^2)^{1/2}}{\pi Eb'}[(\sigma_Y - \sigma_c)I_1 + (\sigma_c - \sigma_{0c})I_2], \tag{A2}$$

where

$$I_1 = \int_{-b}^{b}\frac{dx_1'}{(x_1' - x_1)(x_1'^2 - a^2)^{1/2}}$$

and

$$I_2 = \int_{-c}^{c}\frac{dx_1'}{(x_1' - x_1)(x_1'^2 - a^2)^{1/2}}$$

The integrals I_1 and I_2 exist in the Cauchy sense that they represent the principle value P.V. of the integrals. $f(x)$ is the linear combination of two similar integrals indicating that there is linear superposition of two distribution functions.

It can be shown that

$$f(x_1) = -\frac{4}{\pi E b'}[(\sigma_Y - \sigma_c)I_3 + (\sigma_c - \sigma_{0c})I_4] \quad \text{(A3)}$$

where

$$I_3 = \cosh^{-1}\left(\frac{m_2}{b - x_1} + n_2\right) - \cosh^{-1}\left(\frac{m_2}{b + x_1} + n_2\right)$$

$$I_4 = \cosh^{-1}\left(\frac{m_1}{c - x_1} + n_1\right) - \cosh^{-1}\left(\frac{m_1}{c + x_1} + n_1\right)$$

and

$$m_1 = \frac{a^2 - c^2}{a}, \quad n_1 = \frac{c}{a},$$

$$m_2 = \frac{a^2 - b^2}{a}, \quad n_2 = \frac{b}{a}.$$

The opening displacement at the active zone tip $y(b)$ is given by

$$y(b) = \int_b^a b' f(x_1)\mathrm{d}x_1 . \quad \text{(A4)}$$

Finally one obtains

$$y(b) = \frac{8}{\pi E}(\sigma_Y - \sigma_c)b\ln\frac{a}{b} + \frac{4(\sigma_c - \sigma_{0c})}{E}\left[(b + c)\cosh^{-1}\left(\frac{m_1}{c + b} + n_1\right) - (b - c)\cosh^{-1}\left(\frac{m_1}{c - b} + n_1\right)\right]. \quad \text{(A5)}$$

The second term in equation A5 is much smaller than the first term. Thus as a good approximation

$$y(b) \cong \frac{8}{\pi E}(\sigma_Y - \sigma_c)b\ln\frac{a}{b}. \quad \text{(A6)}$$

The opening displacement at the inert zone tip $y(c)$ is given by

$$y(c) = \int_c^a b' f(x_1)\mathrm{d}x_1 , \quad \text{(A7)}$$

and in the similar approximation

$$y(c) = \frac{8}{\pi E}(\sigma_c - \sigma_{0c})c\ln\frac{a}{c} + \frac{4}{\pi E}(\sigma_Y - \sigma_c)(b - c)\cosh^{-1}\left(\frac{2(a - b)}{b - c} + 1\right). \quad \text{(A8)}$$

Appendix 2

The total craze thickness $t(x_1)$ consists of two contributions

$$t(x_1) = t_0(x_1) + y(x_1), \quad \text{(A9)}$$

where $t_0(x_1)$ is an unextended craze fibrils length drawn from the surrounding bulk and $y(x_1)$ is the total displacement of craze surfaces, see Appendix 1. The drawing ratio λ is defined by

$$\lambda = \frac{t(x_1)}{t_0(x_1)}. \quad \text{(A10)}$$

Usually, $\lambda \approx 4$. Combining Equations A9 and A10 we arrive at

$$t(x_1) = \frac{\lambda}{\lambda - 1}y(x_1). \quad \text{(A11)}$$

Appendix 3

The principal result derived by Rice [35] concerns two distinct load systems symmetrical about the crack line denoted by Q_i and Q_j which induce the stress intensity factors $K^{(i)}(a)$ and $K^{(j)}(a)$, where a is the crack length. It holds

$$\frac{\mathrm{d}C_{ij}}{\mathrm{d}a} = \frac{2}{E}K^{(i)}(a)K^{(j)}(a), \quad \text{(A12)}$$

where the compliances C_{ij} read

$$C_{ij} = \int_\Xi \boldsymbol{t}^{(i)}\boldsymbol{u}^{(j)}\mathrm{d}\Xi, \quad \text{(A13)}$$

with $\boldsymbol{t}^{(i)}$ standing for the stress vector of the loading system Q_i on the boundary Ξ and with $\boldsymbol{u}^{(j)}$ standing for the displacement vector of the loading system Q_j on the boundary Ξ. No body forces are assumed.

Clearly, if Ξ denotes the craze surfaces with the stress component $t_2^{(i)} = \pm\sigma_c$ being non-zero along the craze faces in the interval $x_1 \in \langle c; b\rangle$ and inducing the stress intensity factor $K[\sigma_c]$, and with $u_2^{(j)} = \pm 1/2y(x_1, a)$ being the displacement component of the loading system j inducing the stress intensity factor K', Equation A13 yields

$$C_{ij} = \int_c^b \sigma_c y(x_1, a)\mathrm{d}x_1. \quad \text{(A14)}$$

Substituting Equation A14 into Equation A12 one gets

$$\sigma_c\int_c^b \frac{\partial y(x_1, a)}{\partial a}\mathrm{d}x_1 = \frac{2}{E}K[\sigma_c]K', \quad \text{(A15)}$$

which is Equation 47 used in the main body of the paper.

References

1. G. A. BERNIER and R. P. KAMBOUR, *Macromolecules* **1** (1968) 393.
2. E.J. KRAMER, in "Development in Polymer Fracture-1", edited by E. H. Andrews (Applied Science, London, 1979) p. 55.
3. R. P. KAMBOUR, C. L. GRUNER and E. E. ROMAGOSA, *J. Polym. Sci., Polym. Phys.* Ed. **11** (1973) 1879.
4. J. G. WILLIAMS and G. P. MARSHALL, *Proc. R. Soc. Lond. A* **342** (1975) 55.
5. J. ISRAEL, C. S. KANTAMNENI and W.W. GERBEBICH, in "Mechanical Behaviour of Materials," edited by K. J. Miller and R. F. Smith (Pergamon Press, New York, 1979) p. 393.
6. M. DETTENMAIER and D. LEBERGER, in "Crazing in Polymers Vol. 2", edited by H. H. Kausch (Springer-Verlag, Berlin, Heidelberg, New York, 1990) p. 122.
7. J. BREEN, *J. Mater. Sci.* **28** (1993) 3769.

8. A. N. GENT, *ibid* **5** (1970) 925.
9. E. J. KRAMER and R. A. BUBECK, *J. Polym. Sci., Polym. Phys.* Ed. **16** (1978) 1195.
10. I. M. WARD, "Mechanical Properties of Solid Polymers," 2nd Edn (Wiley Chichester, 1985) p. 375.
11. A. S. ARGON and M. SALAMA, *Mater. Sci. Engng.* **23** (1976) 219.
12. *Idem, Phil. Mag. A* **36** (1977) 1277.
13. G. I. TAYLOR, *Proc. R. Soc. London A* **201** (1950) 192.
14. A. M. DONALD and E. J. KRAMER, *Phil. Mag. A* **43** (1981) 857.
15. R. J. FIELDS and M. F. ASHBY, *ibid* **33** (1976) 33.
16. F. A. McCLINTOCK and A. S. ARGON, "Mechanical Behaviour of Materials" (Addison-Wesley, Reading, Massachusetts, 1966) p. 6.
17. F. A. McCLINTOCK, *J. Appl. Mechanics Trans. ASME* **90** (1968) 363.
18. *Idem.*, in "Physics of Strength and Plasticity", edited by A. S. Argon (MIT Press, Cambridge, Massachusetts, 1969) p. 136.
19. H. R. BROWN and N. G. NJOKU, *J. Polym. Sci., Polym. Phys.* Ed. **36** (1986) 11.
20. E. J. KRAMER, *Adv. Polymer Sci.* **52/53** (1983) 1.
21. A. M. DONALD and E. J. KRAMER, *J. Polym. Sci., Polym. Phys.* Ed. **20** (1982) 899.
22. L. L. BERGER, D. J. BUCKLEY, E. J. KRAMER, H. R. BROWN and R. A. BUBECK, *ibid* **25** (1987) 1670.
23. H. OKAMOTO and Y. OHDE, in "Failure of Plastics", edited by W. Brostow and R. D. Corneliussen (Hanser, Vienna, 1986) p. 330.
24. A. CHUDNOVSKY, I. PALLEY and E. BAER, *J. Mater. Sci.* **16** (1981) 35.
25. A. STOJIMIROVIC and A. CHUDNOVSKY, *Int. J. Fracture* **57** (1992) 281.
26. J. KESTIN and J. R. RICE, in "A critical Review of Thermodynamics", edited by E. B. Stuart, B. Gal-Or and A. J. Brainard (Mono Book Corp., Baltimore 1970) p. 270.
27. L. C. STRUIK, "Physical Aging in Amorphous Polymers and Other Materials" (Elsevier, Amsterdam 1978).
28. P. J. FLORY, "Principles of Polymer Chemistry", (Cornell Univ. Press, Ithaca, New York, 1971).
29. B. D. LAUTERWASSER and E. J. KRAMER, *Phil. Mag. A* **39** (1979) 469.
30. A. S. ARGON, R. E. COHEN, O. S. GEBIZLIOGLU and C. E. SCHWIER, in "Advances in Polymer Science 52/53", edited by H. H. Kausch (Springer Verlag, Berlin, 1983) p. 275.
31. N. VERHEULPEN-HEYMANS and J. C. BAUWENS, *J. Mater. Sci.* **11** (1976) 93.
32. J. D.ESHELBY, in " Fracture Toughness" ISI Publication 121 (The Iron and Steel Institute London, 1968) p. 55.
33. *Idem*, in "Inelastic Behaviour of Solids," edited by M. F. Kanninen, W. F. Adler, A. R. Rosenfield and R. I. Jaffee (Mc Graw-Hill, New York 1970) p. 77.
34. *Idem, J. of Elasticity* **5** (1975) 321.
35. J. R. RICE, *Int. J. Solids Structures* **8** (1972) 751.
36. E. J. KRAMER, *Polymer Engng. Sci.* **24** (1984) 761.

Received 19 September 1994
and accepted 11 December 1995